LAWRENCE
LIVERMORE
NATIONAL
LABORATORY

LLNL-JRNL-667808

The dynamics of equivalent continuums representing truss lattice materials

M. C. Messner, M. I. Barham, M. Kumar, N. R. Barton

February 26, 2015

International Journal of Solids and Structures

Disclaimer

The dynamics of equivalent continuums representing truss lattice materials

Mark C. Messner[a,*], Matthew I. Barham[a], Mukul Kumar[a], Nathan R. Barton[a]

[a]*Lawrence Livermore National Laboratory, P.O. Box 808, L-227, Livermore, CA 94551, USA*

Abstract

Stiffness scales linearly with density in stretch-dominated lattice meta-materials offering the possibility of very light yet very stiff structures. Current additive manufacturing techniques can assemble structures consisting of these lattice materials, but the design of such structures will require accurate, efficient simulation techniques. Equivalent continuum models have several advantages over discrete truss models of stretch dominated lattices, including computational efficiency and ease of model construction. However, the development an equivalent model suitable for representing the dynamic response of a periodic truss is complicated by microinertial effects. This paper derives a dynamic equivalent continuum model for periodic truss structures and verifies it against detailed finite element simulations. The model must incorporate microinertial effects to accurately reproduce long-wavelength characteristics of the response such as anisotropic elastic soundspeeds. The formulation presented here also improves upon previous work by preserving equilibrium at truss joints for affine lattice deformation and by improving numerical stability by eliminating vertices in the effective yield surface.

Keywords: Meta-materials, Micro-mechanics, Additive manufacturing, Dynamic, Trusses

1. Introduction

The development of additive manufacturing (AM) techniques allows the design of both the macroscale and microscale geometry of a structural component (Kruth et al., 1998; Murr et al., 2012; Rosen, 2007). Control over the microgeometry opens up a new design space, effectively allowing the designer to control the properties of a material by varying the material's structure. Cellular lattice materials are a promising class of micro-geometries, offering excellent stiffness-to-weight ratios and simple construction by tiling the periodic unit cell into a macroscale shape (Evans et al., 2001; Warren and Kraynik, 1987). A subclass of lattice materials are stretch dominated lattice materials, where the principal deformation mechanism is axial deformation of the struts. Because the scaling between stiffness and density in these structures is linear they offer the possibility of exceptionally light but stiff materials (Zheng et al., 2014).

The classic structure where deformation occurs through axial stretching and compression of a series of connected struts is the truss. Stretch dominated lattice materials then resemble periodic trusses, albeit on a smaller length scale than the typical structural truss (Hutchinson and Fleck, 2006; Martinsson and Babuška, 2007). Experimental and computational studies of discrete truss structures reveal complicated dynamic behavior, including the existence of band gaps (Howard and Pao, 1998; Signorelli and von Flotow, 1988) and microjetting under impact loading (Winter et al., 2014). Representing these complex phenomena with an equivalent continuum model is challenging. An equivalent continuum model is a material formulation which replaces a periodic discrete structure with a continuum that deforms equivalently under all loads; static and dynamic. Equivalent continuum models have several advantages over discrete simulations: they integrate more easily into existing finite element frameworks; they generally reduce the computational complexity, measured in number of degrees of freedom, required to represent a periodic structure; and they eliminate the difficulty inherent in meshing a complex microgeometry.

This work fills a gap in previous research on modeling periodic truss systems by focusing on the dynamic properties of equivalent continuums. Previous research by Pao et al. (1999); Srikantha Phani et al. (2006) and Yong and Lin (1992) describes models of discrete trusses under dynamic loading. Hutchinson and Fleck (2006) and Mohr (2005) develop equivalent continuum models of trusses under quasi-static loading, which are discussed in more detail subsequently. However, no work to date formulates an equivalent contin-

*Corresponding author. Tel.: +1-925-423-1540
Email address: messner6@llnl.gov (Mark C. Messner)

uum model suitable for representing periodic truss structures undergoing dynamic loading. Such a model must consider the inertial properties of periodic trusses in addition to elastic and plastic properties. Microinertial effects accounting for the actual mechanism of wave propagation through the discrete microstructure become significant when the material is loaded dynamically, for example under impact loading (Fish et al., 2002b,a, 2012; Wang and Sun, 2002). Typically, a model incorporates microinertial effects in order to better represent the dispersion caused by higher order deformation modes. This work demonstrates that a model must consider microinertial effects even to accurately represent the long wavelength response of a periodic truss, even though the long wavelength limit only exercises the lowest deformation modes. Additionally, the equivalent continuum model described here improves upon previous models by developing a formula for the resolved tension in the truss members that better preserves equilibrium at the joints and by eliminating numerical instabilities in the plastic flow rule via a method gleaned from an analogy to crystal plasticity models.

The presentation of the model is organized as follows. Section 2 describes previous equivalent continuum models by Hutchinson and Fleck (2006) and Mohr (2005) and describes the problem of vertices on the effective yield surface. Section 3 derives an equivalent continuum model for periodic truss structures, including microinertial effects. Section 4 verifies the model against quasi-static and dynamic finite element simulations of a discrete octet truss. Finally, Section 5 summarizes the work and describes possible future uses of the model.

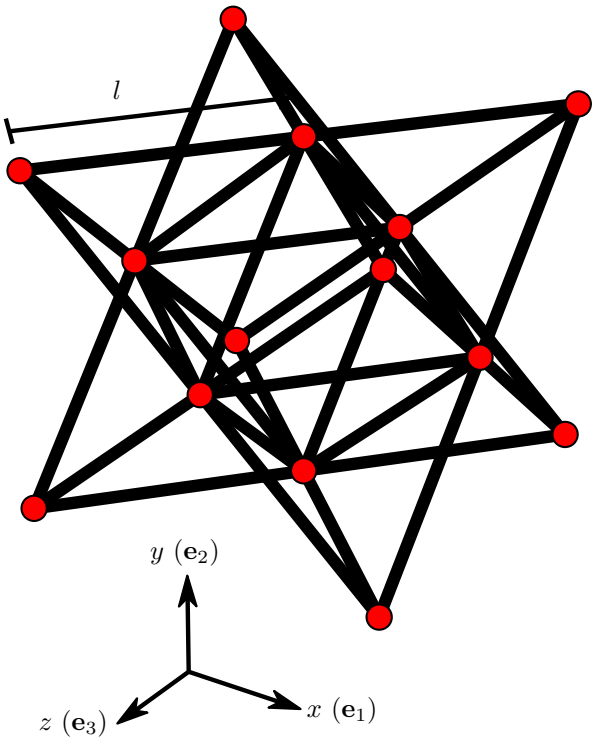

Figure 1: Octet truss unit cell. All struts have equal lengths l. The three lattice vectors have the same length and point in the directions of the indicated cartesian coordinate system. Therefore, the octet truss has a cubic lattice.

2. Quasi-static elastic and plastic equivalent continuum models

A truss is a structural system comprised of joints connected by members called struts. The mechanical assumption of the system is that the joints are structural pins that do not transfer moments and, correspondingly, that the struts transmit only axial forces. In a periodic truss, the combination of a motif and lattice describes the position of all joints. A motif is a collection of vectors describing the position of joints about a common point. Hutchinson and Fleck (2006) refer to each vector as a joint basis vector and the collection of vectors as the joint basis. A lattice is a set of vectors describing the translational symmetry of these common lattice points. The linear combination

$$\mathbf{x}_i = \sum_{k=1}^{n} m_k \mathbf{b}_k \tag{1}$$

describes the position of any lattice point i in a lattice for the set of lattice vectors $\mathbf{b}_k$ and any set of integers m_k. Here n is the dimensionality of the system. Similarly, the position or, equivalently, the connectivity of the struts must also have translational symmetry described by the lattice vectors. Hutchinson and Fleck (2006) describes the position of the struts with a set of vectors called the strut basis. An infinite, periodic truss does not consider boundary effects – the lattice extends to infinity in all directions. A single unit cell, encompassing all the symmetries of the periodic truss, fully describes such a structure. Figure 1 shows one possible unit cell for a periodic octet-truss.

Hutchinson and Fleck (2006) describe a method based on the Bloch wave theory for calculating the effective equivalent elastic tensor for any 2D or 3D periodic truss structure. Their approach is to calculate the sum of the strain energy in all struts in the unit cell for an arbitrary macrostrain field, divide by the unit cell volume to find the strain energy density, and then take the second derivative with respect to the strain to find the effective elastic stiffness tensor. The strain energy density per unit reference volume in an arbitrary, linear elastic

truss with constant Young's moduli is given by

$$\Phi(\boldsymbol{\varepsilon}) = \frac{E}{2V_0} \sum_{i=1}^{n_{bars}} A_i l_i \varepsilon_i^2 \tag{2}$$

where V_0 is the reference unit cell volume, E is the Young's modulus, A_i the strut cross-sectional area, l_i the strut length, and ε_i the axial strain of a strut under a given loading. Assuming the deformation remains affine for all joints, the strain in each strut is

$$\varepsilon_i = \mathbf{n}_i \cdot \boldsymbol{\varepsilon} \cdot \mathbf{n}_i \tag{3}$$

where $\boldsymbol{\varepsilon}$ is the macroscale strain tensor and $\mathbf{n}_i$ the strut normal. Taking the second derivative with respect to strain yields the formula

$$\mathbf{C} = E\bar{\rho}\hat{C}_{ijkl} \tag{4}$$

with

$$\hat{\mathbf{C}} = \sum_{s=1}^{n_{bars}} A_i l_i \mathbf{n}_i \otimes \mathbf{n}_i \otimes \mathbf{n}_i \otimes \mathbf{n}_i / \sum_{i=1}^{n_{bars}} l_i A_i. \tag{5}$$

Here $\bar{\rho}$ is the relative density of the equivalent continuum – the ratio of the density of the truss as a whole to the density of the solid material comprising the struts – assuming the volume of the joints is small. This method and that of Hutchinson and Fleck (2006) produce the same equivalent elasticity tensor for simple lattices – periodic trusses for which a Bravais lattice describes the position of the joints.

Mohr (2005) describes a theory of equivalent continuum plasticity for truss structures. The theory first defines yield criteria for individual struts, for example plastic yielding and elastic buckling. Mohr then defines the yield surface of the equivalent continuum material to be the locus of points in stress space that cause any single strut to yield. Figure 2 shows a 2D slice in stress space of the yield surface this method generates for the octet truss, only considering a single yield state of σ_0 in either compression or tension. In the full stress space, these types of yield surfaces consist of the intersection of hyperplanes, with one hyperplane for each yield criteria in each strut. Associated plastic flow then occurs in directions normal to the yield surface. The problem with this definition of equivalent plasticity is the vertices where multiple hyperplanes intersect. At these points, there is no clearly defined normal to the yield surface and plastic flow becomes degenerate. This causes numerical instability in the implemented plasticity model – a problem which has also been observed in models of plasticity for rate-independent single crystals (Kocks, 1998). The equivalent continuum model developed in this work solves this problem of vertices and also introduces a correction to Mohr's formula for the tension resolved in each strut.

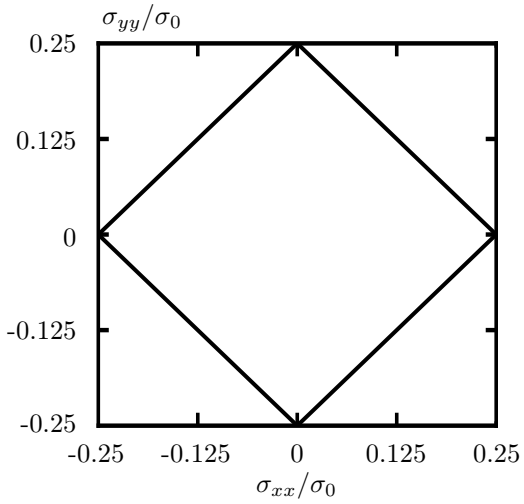

Figure 2: The yield surface of the octet truss for $\bar{\rho} = 0.9$, defined as the locus of strut yield stresses, projected onto the σ_{xx}-σ_{yy} plane.

3. Collapse model

3.1. Pressure sensitive, viscoplastic flow

Consider the unit cell of a periodic truss structure. Neglecting plasticity and given the displacements of the joints a and b defining strut i, the elongation of the strut is

$$e_i = \mathbf{n}_i \cdot (\mathbf{d}_a - \mathbf{d}_b) \tag{6}$$

with $\mathbf{n}_i$ the strut normal, $\mathbf{n}_i = (\mathbf{x}_a - \mathbf{x}_b)/l_i$ with $\mathbf{x_a}$ and $\mathbf{x_b}$ the nodal positions and $l_i = \|\mathbf{x}_a - \mathbf{x}_b\|$, and $\mathbf{d}_a$ and $\mathbf{d}_b$ the displacements of joints a and b, respectively. Assuming a linear relation between engineering strain and stress, the stress in the strut is

$$\sigma_i = \frac{E}{l_i} \mathbf{n}_i \cdot (\mathbf{d}_a - \mathbf{d}_b) \tag{7}$$

with E the Young's modulus of the struts. Assume the Cauchy-Born hypothesis with a simple lattice. Then the displacement of any joint in the periodic truss under an applied macroscopic strain field $\boldsymbol{\varepsilon}(\mathbf{x})$ is affine and given by

$$\mathbf{d}_a = \boldsymbol{\varepsilon} \cdot \mathbf{x}_a. \tag{8}$$

Now consider plasticity. Additively decompose the strain into elastic and plastic parts $\boldsymbol{\varepsilon} = \boldsymbol{\varepsilon}^e + \boldsymbol{\varepsilon}^p$. Equation 8 becomes

$$\mathbf{d}_a = (\boldsymbol{\varepsilon}^e + \boldsymbol{\varepsilon}^p) \cdot \mathbf{x}_a = \mathbf{d}_a^e + \mathbf{d}_a^p \tag{9}$$

with $\mathbf{d}_a^e := \boldsymbol{\varepsilon}^e \cdot \mathbf{x}_a$ and $\mathbf{d}_a^p := \boldsymbol{\varepsilon}^p \cdot \mathbf{x}_a$. Assume that only elastic strut displacements cause stress in Eq. 7. Section 2 shows, based on Hutchinson and Fleck (2006), that the relation between stress and elastic strain for any periodic truss comprised of

struts with the same elastic stiffness, but possibly different areas, is

$$\boldsymbol{\sigma} = \bar{\rho} E \hat{\mathbf{C}} : \boldsymbol{\varepsilon}^e \tag{10}$$

where $\hat{\mathbf{C}}$ is a unitless second order tensor which depends on the strut lengths and areas and the truss topology. Inverting Eq. 10 and combining with Eqs. 7 and 8 yields a formula relating macroscale stress to the strut tension:

$$\sigma_i = \frac{1}{\bar{\rho}} \mathbf{n}_i \cdot \hat{\mathbf{C}}^{-1} : \boldsymbol{\sigma} \cdot \frac{\mathbf{x}_a - \mathbf{x}_b}{l_i} \tag{11}$$

Recognizing that $\mathbf{n}_i = \frac{\mathbf{x}_a - \mathbf{x}_b}{l_i}$ and rearranging the equation yields:

$$\sigma_i = \frac{1}{\bar{\rho}} \left(\mathbf{n}_i \otimes \mathbf{n}_i \right) : \hat{\mathbf{C}}^{-1} : \boldsymbol{\sigma} \tag{12}$$

Note the strong similarity of this equation to Eq. 13 of Mohr (2005):

$$\sigma_i = \frac{1}{c_i} \boldsymbol{\sigma} : \left(\mathbf{n}_i \otimes \mathbf{n}_i \right) \tag{13}$$

with c_i the volume fraction of the strut. See Fig. 3 for examples of the different load distributions generated for an octet truss by these two different strut tension expressions. Consider the circled joint for the uniaxial load case. Three struts meet at this joint with strut normals $\mathbf{n}_1 = \sqrt{2}/2\mathbf{g}_1 + \sqrt{2}/2\mathbf{g}_3$, $\mathbf{n}_2 = \sqrt{2}/2\mathbf{g}_2 + \sqrt{2}/2\mathbf{g}_3$, and $\mathbf{n}_3 = \sqrt{2}/2\mathbf{g}_1 + \sqrt{2}/2\mathbf{g}_2$, with $\mathbf{g}_i$ the basis vectors of the cartesian coordinate system shown in the figure. This joint is also subjected to the force resulting from the imposed uniaxial σ_{xx} in direction $\mathbf{n}_4 = \mathbf{g}_1$. As the figure shows, calculating the strut tensions via Eq. 13 and writing the resulting nodal equilibrium equation yields

$$\mathbf{0} = f_1 \mathbf{n}_1 + 0\mathbf{n}_2 + f_3 \mathbf{n}_3 + f_4 \mathbf{n}_4, \tag{14}$$

i.e. zero force in strut with normal $\mathbf{n}_2$. Summing forces in the y-direction ($\mathbf{g}_2$) shows that this joint cannot be in equilibrium. However, Eq. 12 correctly generates a compressive force in the strut with normal $\mathbf{n}_2$, satisfying the nodal equilibrium condition. This is a general feature of Eq. 12, provided the lattice topology is simple, because the stress state assumed by Eqs. 4 and 5 minimizes the internal energy. For complex lattices these equations would have to be modified to account for internal degrees of freedom. Equation 12 would still preserve equilibrium, but the unitless topology tensor $\hat{\mathbf{C}}$ would now depend on the current strain $\boldsymbol{\varepsilon}$, requiring iteration to solve for the equilibrium strut stresses.

Equation 12 also resembles the expression for calculating the shear resolved along a single system in a crystal plasticity model (see, for example Asaro 1983). Section 2 described the yield surface of periodic trusses and observed the degeneracy of plastic flow at yield surface vertices. Models of grain-scale plasticity in metals, for example the Taylor-Bishop-Hill theory of rate-independent, single FCC crystal plasticity, encounter the same problem (Bishop and Hill, 1951b,a). The solution typically adopted by crystal plasticity models is to make the yield surface moderately rate-sensitive (Kocks, 1998). Adopting this approach for periodic trusses smooths the yield surface at the intersection of the hyperplanes representing strut limit states (see Fig. 2), preventing degenerate flow at the vertices. Plastic flow in actual materials is at least somewhat rate sensitive, so at the worst introducing a moderate rate sensitivity into the model simply overestimates the physical rate sensitivity.

There is a fundamental similarity between crystal plasticity models and equivalent truss models – both seek to describe the deformation of lattice materials. In crystal models the material consists of individual atoms positioned in a lattice. For a truss model, the lattice consists of the joints. The key differences between the two types of models is the deformation mechanism under consideration – for crystals shear along crystallographic planes; for trusses axial deformation along the struts. Nevertheless, the final systems of equations of the two models are very similar.

For small deformations, the elastic tensor relates the rate of elastic strain to the stress rate:

$$\dot{\boldsymbol{\sigma}} = \frac{\dot{\bar{\rho}}}{\bar{\rho}} \boldsymbol{\sigma} + \bar{\rho} E \hat{\mathbf{C}} : \left(\dot{\boldsymbol{\varepsilon}} - \dot{\boldsymbol{\varepsilon}}^p \right). \tag{15}$$

Following the ideas of crystal plasticity kinematics, the plastic strain rate is an additive composition of uniaxial strains along each strut in the truss unit cell:

$$\dot{\boldsymbol{\varepsilon}}^p = \sum_{i=1}^{n_{bars}} \dot{\varepsilon}_i \left(\mathbf{n}_i \otimes \mathbf{n}_i \right). \tag{16}$$

The uniaxial strain rate along each strut varies with the tensile stress in the strut viscoplastically:

$$\dot{\varepsilon}_i = \dot{\varepsilon}_0 \left| \frac{\sigma_i}{\bar{\sigma}_i} \right|^{n-1} \frac{\sigma_i}{\bar{\sigma}_i} \tag{17}$$

where σ_i is the strut stress, defined by Eq. 12, $\bar{\sigma}_i$ the uniaxial strut flow stress, $\dot{\varepsilon}_0$ a reference strain rate, and n the rate-sensitivity parameter. This expression is essentially identical to the resolved shear/slip equation commonly adopted for crystal plasticity models (see, for example, Roters et al., 2010) but replaces shear stress and strain with tensile stress and strain. Let $\dot{\varepsilon}_0 = \sqrt{2/3 \dot{\boldsymbol{\varepsilon}} : \dot{\boldsymbol{\varepsilon}}}$, the effective strain rate, and use $n = 20$ for low-to-moderate rate sensitivity.

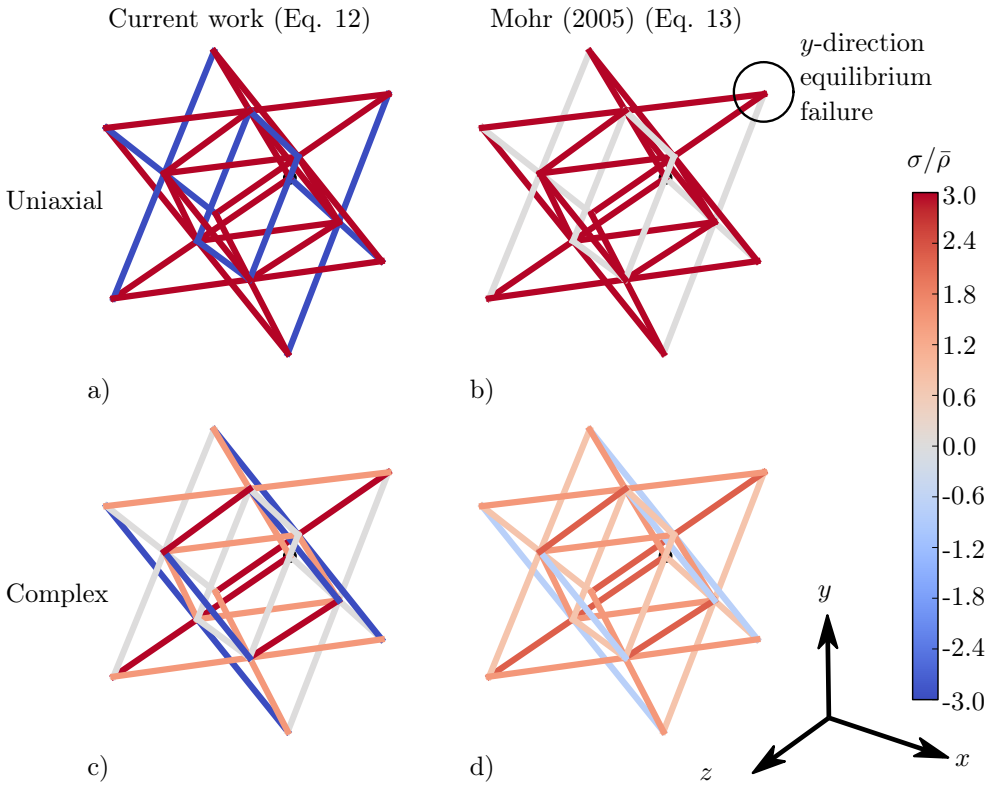

Figure 3: Strut tensions from the two different strut tension formulas (Eq. 12 from this work and Eq. 13 from Mohr, 2005) for an octet truss under two different stress states. State "Uniaxial" is uniaxial, x-direction tension ($\begin{bmatrix} \sigma & 0 & 0 & 0 & 0 & 0 \end{bmatrix}$) and state "Complex" is a combination of biaxial x-y tension and xz shear ($\begin{bmatrix} \sigma/4 & \sigma/4 & 0 & 0 & \sigma/4 & 0 \end{bmatrix}$). The formula from Mohr develops non-equilibrium strut tensions, as demonstrated for the y-direction of the indicated joint for the uniaxial loading.

In general the model can track the flow stress separately in each strut. This requires maintaining a history variable for each strut. To reduce the computational expense of tracking and updating these variables the formulation adopts, again from crystal plasticity, the idea of isotropic hardening:

$$\dot{\bar{\sigma}}_i = \dot{\bar{\sigma}} = H \sum_{i=1}^{n_{bars}} |\dot{\varepsilon}_i| \tag{18}$$

$$\bar{\sigma}\left(t=0\right) = \sigma_0$$

where σ_0 is the yield stress of the struts and H the hardening modulus.

While these expressions are for small deformations, the similarity of Eqs. 12, 15, 16, 17, and 18 to their crystal plasticity counterparts means methods of extending crystal plasticity kinematics to large deformations apply equally well to the periodic truss equations, provided the deformation remains affine. For example, methods of computing and applying the large rotations for crystal plasticity (e.g. Hill and Rice (1972); Forest and Pilvin (1999); Messner et al. (2015)) also apply to the periodic truss. Even the interpretation of these rotations is similar between the two models: in crystal plasticity large rotations represent the deformation of the atomic lattice, in the periodic truss model they represent the deformation of the lattice of truss joints. This analogy breaks down with the presence of internal degrees of freedom (complex lattices). In this case, the updated joint positions would require explicit consideration of internal equilibrium. The updated joint coordinates, including rotations, could be calculated by minimizing the strain energy as a function of the position of the internal degrees of freedom.

These expressions only define the constitutive response of the periodic truss at a constant value of relative density. To study the dynamic collapse of periodic truss structures the equations must be supplemented by an evolution equation for the relative density $\bar{\rho}$. Since $\bar{\rho} = \frac{V_m}{V}$ where V_m is the volume of the truss material and V the total volume the rate-of-change of the relative density is $\dot{\bar{\rho}} = \frac{\dot{V}_m}{V} - \frac{V_m}{V^2}\dot{V}$. Assuming the truss material remains approximately incompressible compared to the equivalent continuum as a whole and neglecting elastic volume change:

$$\dot{\bar{\rho}} = -\bar{\rho}\frac{\dot{V}}{V} = -\bar{\rho}\,\mathrm{tr}\,\dot{\varepsilon}^p. \tag{19}$$

A coupled, implicit integration of Eqs. 15, 18, and 19 supplemented by Eqs. 12, 16, and 18 define the model. Algorithm 1 summarizes the stress update procedure. In the algorithm, Eq. 12 defines the strut tensions σ_i. The appendix details the Jacobian function required in the material update.

Algorithm 1 Stress update procedure for the periodic truss model.

function UPDATE($\Delta\boldsymbol{\varepsilon}_{n+1}$, $\boldsymbol{\sigma}_n$, $\bar{\sigma}_n$, $\bar{\rho}_n$)
  $\mathbf{x} \leftarrow \begin{bmatrix} \boldsymbol{\sigma}_n & \bar{\sigma}_n & \bar{\rho}_n \end{bmatrix}$
  $\Delta\varepsilon_0 \leftarrow \sqrt{2/3\Delta\boldsymbol{\varepsilon}_{n+1} : \Delta\boldsymbol{\varepsilon}_{n+1}}$
  while $\|\mathbf{R}\| > tol$ **do**
    $\Delta\boldsymbol{\varepsilon}^p \leftarrow \sum_{i=1}^{n_{bars}} \Delta\varepsilon_0 \left|\frac{\sigma_i}{\bar{\sigma}}\right|^{n-1} \frac{\sigma_i}{\bar{\sigma}} \left(\mathbf{n}_i \otimes \mathbf{n}_i\right)$
    $\mathbf{R}_\sigma \leftarrow \left(1 + \mathrm{tr}\,\Delta\boldsymbol{\varepsilon}^p\right)\boldsymbol{\sigma} - \boldsymbol{\sigma_n} - \bar{\rho}E\hat{\mathbf{C}} \cdot \left(\Delta\boldsymbol{\varepsilon}_{n+1} - \Delta\boldsymbol{\varepsilon}^p\right)$
    $R_{\bar{\sigma}} \leftarrow \bar{\sigma} - \bar{\sigma}_n - H\sum_{i=1}^{n_{bars}} \Delta\varepsilon_0 \left|\frac{\sigma_i}{\bar{\sigma}}\right|^n$
    $R_{\bar{\rho}} \leftarrow \bar{\rho} - \bar{\rho}_n + \bar{\rho}\,\mathrm{tr}\,\Delta\boldsymbol{\varepsilon}^p$
    $\mathbf{R} \leftarrow \begin{bmatrix} \mathbf{R}_\sigma & R_{\bar{\sigma}} & R_{\bar{\rho}} \end{bmatrix}$
    $\mathbf{J} \leftarrow$ JACOBIAN($\boldsymbol{\sigma}, \bar{\sigma}, \bar{\rho}, \Delta\boldsymbol{\varepsilon}_{n+1}$)
    $\Delta\mathbf{x} \leftarrow -\mathbf{J}^{-1} \cdot \mathbf{R}$
    $\mathbf{x} \leftarrow \mathbf{x} + \Delta\mathbf{x}$
    $\begin{bmatrix} \boldsymbol{\sigma} & \bar{\sigma} & \bar{\rho} \end{bmatrix} \leftarrow \mathbf{x}$
  end while
  return $\boldsymbol{\sigma}$, $\bar{\sigma}$, $\bar{\rho}$
end function

3.2. Inertial effects

3.2.1. Derivation

In the absence of an applied body force, the equation

$$\mathbf{f}_{interia} + \mathbf{f}_{internal} = \mathbf{0} \tag{20}$$

summarizes the conservation of linear momentum. Here

$$\mathbf{f}_{internal} = \boldsymbol{\nabla} \cdot \boldsymbol{\sigma}\left(\boldsymbol{\varepsilon}\right) \tag{21}$$

gives the internal body force, with $\boldsymbol{\sigma}\left(\boldsymbol{\varepsilon}\right)$ the stress/strain relation derived above. The inertial force in the struct normal direction for a single strut is:

$$f_i = \int_0^{l_i} \rho_B A_i \ddot{u}_i\left(\xi_i\right) d\xi_i. \tag{22}$$

Assuming small deformations and a simple lattice, the Cauchy-Born assumption gives the joint accelerations as a function of the second time derivative of the applied strain

$$\ddot{\mathbf{u}} = \ddot{\boldsymbol{\varepsilon}} \cdot \mathbf{x}. \tag{23}$$

Using $\ddot{u}_i = \ddot{\mathbf{u}} \cdot \mathbf{n}_i$ and Eq. 22, the contribution of a single strut to the inertial force of the periodic structure is

$$\mathbf{f}_i = \left(\int_0^{l_i} \rho_B A_i \mathbf{n}_i \cdot \ddot{\boldsymbol{\varepsilon}} \cdot \mathbf{x} d\xi_i\right) \mathbf{n}_i \tag{24}$$

including vector direction.

The inertial body force of the the homogenized truss is the volume-average of the contributions of each strut in the unit cell:

$$\mathbf{f}_{inertia} = \frac{\rho_B}{V} \int_V \left(\int_0^{l_i} A_i \mathbf{n}_i \cdot \ddot{\boldsymbol{\varepsilon}} \cdot \mathbf{x} d\xi_i\right) \mathbf{n}_i dV. \tag{25}$$

The field variables are constant in the line integral over the struts:

$$\mathbf{f}_{inertia} = \frac{\rho_B}{V} \int_V \ddot{\boldsymbol{\varepsilon}} \cdot \mathbf{x} \cdot \left\{ \int_0^{l_i} A_i \left(\mathbf{n}_i \otimes \mathbf{n}_i \right) d\xi_i \right\} dV \tag{26}$$

$$\mathbf{f}_{inertia} = \frac{\rho_B}{V} \int_V l_i A_i \ddot{\boldsymbol{\varepsilon}} \cdot \mathbf{x} \cdot \left(\mathbf{n}_i \otimes \mathbf{n}_i \right) dV \tag{27}$$

The spatial gradient of Eq. 23 gives

$$\boldsymbol{\nabla} \ddot{\mathbf{u}} = \boldsymbol{\nabla} \ddot{\boldsymbol{\varepsilon}} \cdot \mathbf{x} + \ddot{\boldsymbol{\varepsilon}}. \tag{28}$$

Therefore, in the first-order approximation (for a constant macrostrain field):

$$\boldsymbol{\nabla} \ddot{\mathbf{u}} = \ddot{\boldsymbol{\varepsilon}}. \tag{29}$$

By integration by parts, Eq. 27 becomes

$$\mathbf{f}_{inertia} = \frac{\rho_B}{V} \left\{ \int_{\partial V} l_i A_i \left(\ddot{\mathbf{u}} \cdot \hat{\mathbf{n}} \right) \hat{\mathbf{n}} \cdot \left(\mathbf{n}_i \otimes \mathbf{n}_i \right) dS - \int_V l_i A_i \ddot{\mathbf{u}} \cdot \left(\mathbf{n}_i \otimes \mathbf{n}_i \right) dV \right\} \tag{30}$$

with $\hat{\mathbf{n}}$ the surface normal of the unit cell. The requirement of periodicity implies $\int_{\partial V} l_i A_i \left(\ddot{\mathbf{u}} \cdot \hat{\mathbf{n}} \right) \hat{\mathbf{n}} \cdot \left(\mathbf{n}_i \otimes \mathbf{n}_i \right) dS = 0$ leaving the expression:

$$\mathbf{f}_{inertia} = -\frac{\rho_B}{V} \int_V l_i A_i \ddot{\mathbf{u}} \cdot \left(\mathbf{n}_i \otimes \mathbf{n}_i \right) dV \tag{31}$$

Expressing the volume integral as a sum over the finite struts:

$$\mathbf{f}_{inertia} = -\left\{ \frac{\rho_B}{V} \sum_{i=1}^{n_{bars}} l_i A_i \left(\mathbf{n}_i \otimes \mathbf{n}_i \right) \right\} \cdot \ddot{\mathbf{u}}. \tag{32}$$

Rearranging Eq. 32 yields the equation

$$\mathbf{f}_{interia} = \rho \ddot{\mathbf{u}} - \frac{\rho_B}{V} \sum_{i=1}^{n_{bars}} l_i A_i \left(\mathbf{I} - \mathbf{n}_i \otimes \mathbf{n}_i \right) \cdot \ddot{\mathbf{u}} \tag{33}$$

which expresses the inertial force as the macroinertia minus a microinertial correction term.

Using Eq. 29 and expanding the volume integral into a sum over the struts, Eq. 27 can also be expressed as

$$\mathbf{f}_{inertia} = \rho \ddot{\mathbf{u}} - \boldsymbol{\nabla} \cdot \left\{ \frac{\rho_B}{V} \sum_{i=1}^{n_{bars}} l_i A_i \left(\mathbf{I} - \mathbf{n}_i \otimes \mathbf{n}_i \right) \cdot \ddot{\boldsymbol{\varepsilon}} \right\}. \tag{34}$$

With this form the balance of linear momentum can be expressed as

$$\rho \ddot{\mathbf{u}} = \boldsymbol{\nabla} \cdot \left\{ \boldsymbol{\sigma} \left(\boldsymbol{\varepsilon} \right) + \frac{\rho_B}{V} \sum_{i=1}^{n_{bars}} l_i A_i \left(\mathbf{I} - \mathbf{n}_i \otimes \mathbf{n}_i \right) \cdot \ddot{\boldsymbol{\varepsilon}} \right\}, \tag{35}$$

meaning the microinertial correction can be applied as a fictitious stress instead of a modification to the standard inertial force:

$$\rho \ddot{\mathbf{u}} = \boldsymbol{\nabla} \cdot \left\{ \boldsymbol{\sigma} \left(\boldsymbol{\varepsilon} \right) + \boldsymbol{\sigma}_\mu \left(\ddot{\boldsymbol{\varepsilon}} \right) \right\}. \tag{36}$$

The microinertial term developed here specifically for a truss lattice material resembles the result of applying the general theory developed by Fish et al. (2002b,a) and Fish et al. (2012) to the periodic truss system.

3.2.2. Implementation of the microinertial correction

Depending on the application, there may be advantages to implementing either Eq. 33 or Eq. 36.

Equation 33 is preferable when calculating the elastic wavespeeds in the homogenized truss via the Christoffel equation. The standard eigenvalue problem

$$\left(C_{ijkl} n_j n_l - \omega^2 \rho \delta_{ik} \right) p_k = 0 \tag{37}$$

with C_{ijkl} the (effective) elastic stiffness, n_j the direction, ω the frequency, and p_k the polarization vector becomes the generalized eigenvalue problem

$$\left(C_{ijkl} n_j n_l - \omega^2 M_{ik} \right) p_k = 0 \tag{38}$$

with $M_{ik} = \frac{\rho_B}{V} \sum_{s=1}^{n_{bars}} l^{(s)} A^{(s)} n_i^{(s)} n_j^{(s)} \ddot{u}_{jk}$.

For implicit finite elements Eq. 32 may also be preferable. The inertial term (mass matrix) of the standard, implicit Galerkin discretization for the unknown accelerations $\ddot{d}_j$ with shape functions N_{ij}

$$\mathbf{f}_{inertia} = \int_\Omega \rho N_{ik} N_{kj} d\Omega \ddot{d}_j \tag{39}$$

becomes

$$\mathbf{f}_{inertia} = \int_\Omega \rho N_{ik} G_{kl} N_{lj} d\Omega \ddot{d}_j \tag{40}$$

with

$$\mathbf{G} = \frac{\rho_B}{V_{cell}} \sum_{i=1}^{n_{bars}} l_i A_i \left(\mathbf{n}_i \otimes \mathbf{n}_i \right). \tag{41}$$

Therefore, implementing the microinertial correction requires only changing the definition of the mass matrix.

In explicit finite element formulations or in implicit finite element implementations where altering the mass matrix is difficult Eq. 36 becomes preferable. In these situations the microinertial correction can be implemented as a fictitious stress calculated during the material stress update. At a minimum, a finite element framework will provide a material model with the strain at the new and previous time steps and the set of history variables at the previous time step. The model must return the updated stress:

$$\boldsymbol{\sigma}_{n+1} = \boldsymbol{\sigma} \left(\boldsymbol{\varepsilon}_{n+1}, \boldsymbol{\varepsilon}_n, \mathbf{s}_n \right). \tag{42}$$

To implement the microinertial correction the material model instead returns

$$\boldsymbol{\sigma}_{n+1} = \boldsymbol{\sigma}\left(\boldsymbol{\varepsilon}_{n+1}, \boldsymbol{\varepsilon}_n, \mathbf{s}_n\right) + \frac{\rho_B}{V} \sum_{i=1}^{n_{bars}} l_i A_i \left(\mathbf{I} - \mathbf{n}_i \otimes \mathbf{n}_i\right) \cdot \ddot{\boldsymbol{\varepsilon}}_{n+1}. \quad (43)$$

The update requires the second time derivative of the strain $\ddot{\boldsymbol{\varepsilon}}_{n+1}$, typically not available to a FE material model. The material model could construct the time derivative via the differencing scheme

$$\ddot{\boldsymbol{\varepsilon}}_{n+1} = \frac{\dot{\boldsymbol{\varepsilon}}_{n+1} - \dot{\boldsymbol{\varepsilon}}_n}{\Delta t_{n+1}}. \quad (44)$$

This scheme requires the rate of strain at the previous time step as an additional history variable. If the finite element formulation does not provide the strain rate, it can be calculated again by differencing as

$$\dot{\varepsilon}_{n+1} = \frac{\varepsilon_{n+1} - \varepsilon_n}{\Delta t_{n+1}}. \quad (45)$$

4. Example analyses: the octet truss

In this work the octet truss (Fuller, 1961) serves as an exemplar for stretch-dominated lattice materials. Previous research describes the elastic and plastic properties of periodic octet truss structures (Deshpande et al., 2001; Elsayed and Pasini, 2010). Figure 1 shows the unit cell of the octet truss geometry. The direct lattice vectors correspond to the cartesian coordinate system shown on the figure. Consider an infinite, periodic octet truss comprised of struts of equal cross-sectional area A and Young's modulus E. The approximate relative density of this truss is:

$$\bar{\rho} = \frac{6\sqrt{2}A}{l^2}. \quad (46)$$

Following the procedure summarized in Section 2 leads to the effective elastic stiffness (in Voigt notation):

$$\boldsymbol{\sigma} = \mathbf{C} \cdot \boldsymbol{\varepsilon} \quad (47)$$

$$\begin{bmatrix} \sigma_{11} \\ \sigma_{22} \\ \sigma_{33} \\ \sigma_{23} \\ \sigma_{13} \\ \sigma_{12} \end{bmatrix} = E\bar{\rho} \begin{bmatrix} \frac{1}{6} & \frac{1}{12} & \frac{1}{12} & 0 & 0 & 0 \\ \frac{1}{12} & \frac{1}{6} & \frac{1}{12} & 0 & 0 & 0 \\ \frac{1}{12} & \frac{1}{12} & \frac{1}{6} & 0 & 0 & 0 \\ 0 & 0 & 0 & \frac{1}{12} & 0 & 0 \\ 0 & 0 & 0 & 0 & \frac{1}{12} & 0 \\ 0 & 0 & 0 & 0 & 0 & \frac{1}{12} \end{bmatrix} \begin{bmatrix} \varepsilon_{11} \\ \varepsilon_{22} \\ \varepsilon_{33} \\ 2\varepsilon_{23} \\ 2\varepsilon_{13} \\ 2\varepsilon_{12} \end{bmatrix} \quad (48)$$

Property	Description	Value
E	Young's modulus	1780 MPa
ν	Poisson's ratio	0.35
σ_0	Yield stress	40 MPa
H	Hardening modulus	100 MPa
ρ_B	Strut density	1.18 g/cm^3

Table 1: Material properties for the finite element simulations and (excepting Poisson's ratio ν) the equivalent continuum truss model.

and the procedure described in Section 3.2 produces the inertial body force, including microinertial terms:

$$\mathbf{f}_{inertia} = \rho_B \bar{\rho} \begin{bmatrix} \frac{1}{3} & 0 & 0 \\ 0 & \frac{1}{3} & 0 \\ 0 & 0 & \frac{1}{3} \end{bmatrix} \cdot \ddot{\mathbf{u}} \quad (49)$$

where ρ_B is the bulk density of the strut material. Note for this particular periodic truss the inertial force can be expressed as

$$\mathbf{f}_{inertia} = \frac{1}{3}\rho_B \bar{\rho} \ddot{\mathbf{u}}. \quad (50)$$

The physical mass density of the infinite truss is $\rho = \rho_B \bar{\rho}$. Therefore, the effective inertial density of the truss is one-third of its physical mass density – with microinertial effects generating the difference between the physical and effective inertial density. Implementing the microinertial correction to the octet truss requires only reducing the inertial density of the equivalent continuum by two-thirds.

The stiffness matrix (Eq. 48) of the octet truss has cubic symmetry. This implies the elastic properties of the octet truss are anisotropic. The plastic response of the octet is similarly anisotropic. Therefore, the results presented below depend on the orientation of the octet relative to the applied loading. All the load cases described below are uniaxial deformations after rotation of the truss. A crystallographic-type system describes the orientation of the octet after rotation. Figure 1 shows a 100 orientation. A 110 orientation rotates the octet so that the image of the x-axis lies along the line described by $\mathbf{g}_1 + \mathbf{g}_2$ in the original coordinates. Similarly, a 111 orientation rotates the octet so that the image of the x-axis lies along the line described by $\mathbf{g}_1 + \mathbf{g}_2 + \mathbf{g}_3$ in the original coordinates.

4.1. Static analysis

Figure 4 shows one of three meshes used to verify the equivalent continuum model described in this work against detailed finite element models in quasi-static conditions. The three meshes have the same basic structure but vary the radius of the struts to change the overall relative

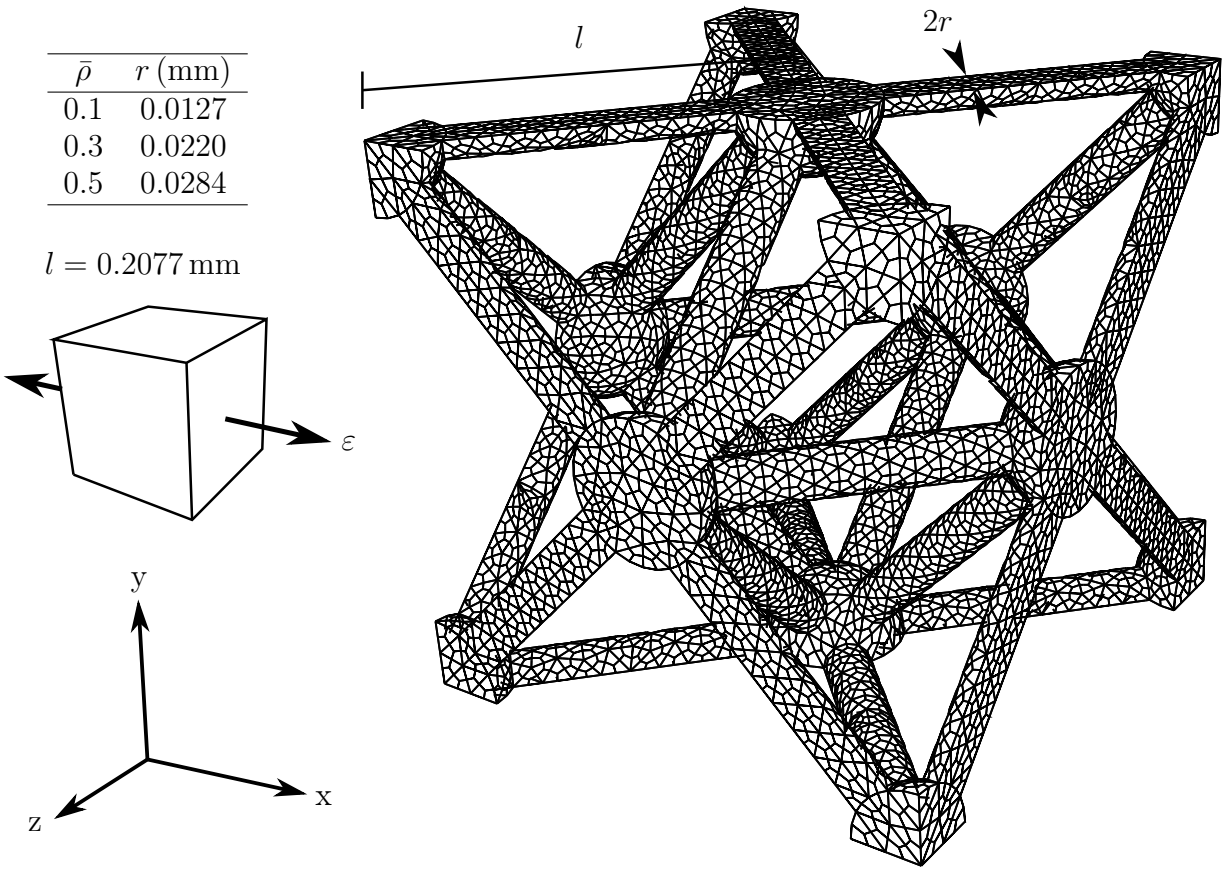

Figure 4: One of three meshes used for verifying the quasi-static properties of the reduced model against full finite element simulations. For all simulations $l = 0.2077\,\mathrm{mm}$, which also fixes the size of the unit cell. Each simulation has a different strut radius r to target a particular value of relative density ($\bar{\rho}$). Changing the strut radius affects the discretization, but all meshes have approximately 30,000 elements and nodes.

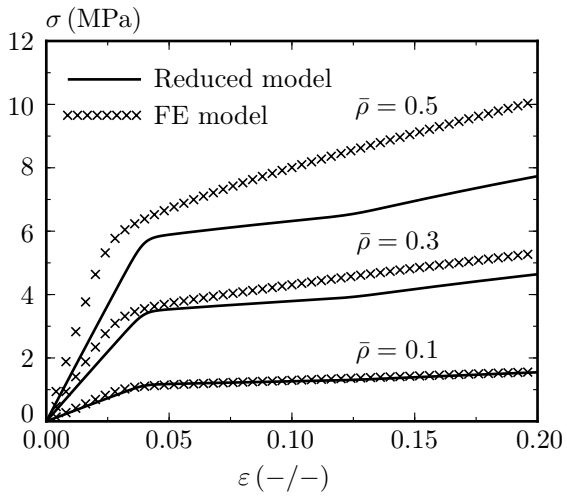

Figure 5: Uniaxial deformation, 100-direction tension stress/strain curves for the octet truss at different relative densities. The plot compares the reduced model developed here to full finite element simulations of an octet truss unit cell.

density of the unit cell ($\bar{\rho}$=0.1,0.3,0.5.) The FE models are loaded with applied displacements in the x-direction and are under symmetry boundary conditions in the y- and z-directions. The FE analyses are run with WARP3D, an open-source, implicit Lagrangian, nonlinear finite element program (`http://www.warp3d.net/`). The equivalent applied strain is

$$\varepsilon = \frac{\Delta d_{applied}}{s} \tag{51}$$

with $d_{applied}$ the applied displacement and s the length of the unit cell, here $s = \sqrt{2}l = 0.294\,\text{mm}$. Define the equivalent stress as the volume average of the stress in each element over the total unit cell

$$\boldsymbol{\sigma} = \frac{1}{V}\int_{\Omega} \boldsymbol{\sigma}_e dV. \tag{52}$$

The material model at all elements in the FE simulation is bilinear plasticity, with Young's modulus E, Poisson's ratio ν, yield stress σ_0, and plastic hardening modulus H. Table 1 summarizes the material properties.

For direct comparison to the FE models, the material model described in this work is driven with the (Voigt notation) strain vector

$$\boldsymbol{\varepsilon} = \begin{bmatrix} \varepsilon & 0 & 0 & 0 & 0 & 0 \end{bmatrix}. \tag{53}$$

The material properties are the same as for the FE simulations, listed in Table 1, except the Poisson's ratio ν is not a parameter of the equivalent truss model.

Figure 5 shows a series of stress-strain curves comparing the equivalent continuum model to the finite element simulations. At low values of relative density the equivalent continuum model agrees with the FE results. As the relative density of the truss increases the equivalent continuum model becomes less and less accurate. Figure 6 explains this trend. The figure shows the axial stress in a strut of the finite element model for the three different values of relative density. The equivalent model assumes the structure behaves as an ideal truss – that bending deformation does not occur in the struts. As Fig. 6 shows, this assumption holds at lower values of relative density where the slenderness of the struts l/r remains high. The normal stress profile for $\bar{\rho} = 0.1$ is nearly a horizontal line – implying zero bending. As the slenderness of the struts decreases the amount of bending increases. This invalidates the assumption of the equivalent continuum truss model and produces the loss of accuracy shown in Fig. 5. This increase in bending stress shows that labeling the octet truss geometry as stretch-dominated must also include the caveat that the slenderness of the struts remains large or, equivalently, the relative density remains low. For practical truss structures assembled by additive manufacturing processes the relative density is small, typically less than $\bar{\rho} = 0.25$. In this range the lattice deforms mostly by stretching, the assumptions of truss theory are valid, and the equivalent continuum model proposed in this work remains accurate.

Figure 7 shows the effect of truss orientation on the quasi-static stress-strain curves generated by the equivalent continuum model. Both the elastic and plastic properties are anisotropic. In the elastic regime, the 111 orientation has the highest stiffness, followed by the 110, and 100 orientations. This follows from the structure of the cubic equivalent elasticity tensor and the general tend has been observed by other researchers (Deshpande et al., 2001; Johnston et al., 2006). For plasticity the directional effects are more complicated. The 100 orientation has the highest yield stress followed by the 111 and 110 orientations. Examining the rotation of the struts relative to the applied loading for each different truss orientation reveals the cause of this trend in the yield stress. In the 110 orientation a family of struts aligns directly with the loading axis, resolving a large amount of strut tension. This causes those struts to yield under comparatively little applied load, decreasing the macroscale, equivalent yield stress. In the 100 orientation all struts are substantially misaligned with the applied loading, resolving relatively little tension and requiring more applied load to yield. The orientation of the truss also effects the slope of the macroscale hardening curve. Load redistribution in the struts can cause a kink in the hardening curve. For the 111 orienta-

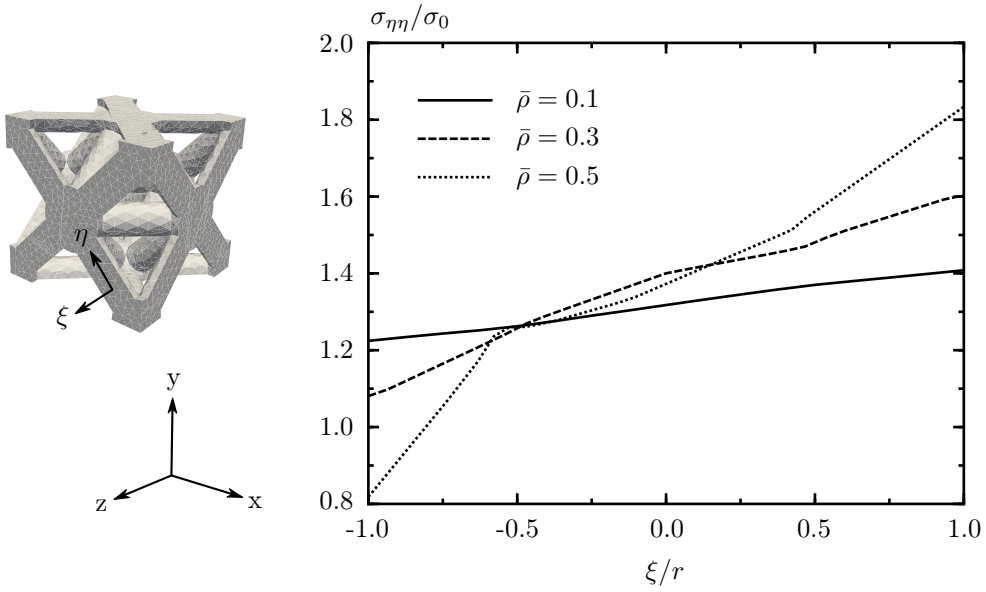

Figure 6: Axial stress ($\sigma_{\eta\eta}$) in the finite element models, normalized by the bulk yield stress $\sigma_0 = 40\,\text{MPa}$, versus position across the strut, normalized by the strut radius, for three different values of relative density. The bending neutral axis is at $\xi = 0$. The coordinate system is positioned at the quarter point of the indicated strut. The amount of bending in the strut increases as the relative density of the truss increases.

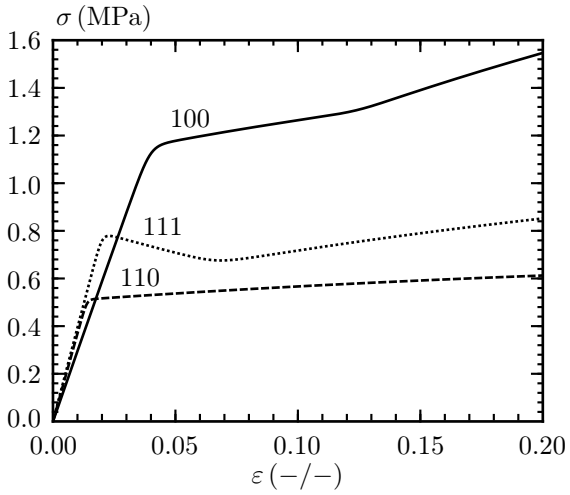

Figure 7: Uniaxial deformation stress/strain curves for the octet truss in three different directions: 100, 110, and 111.

tion load redistribution actually causes macroscale softening, before additional redistribution returns the curve to hardening.

4.2. Hugoniot curves for planar impact

Figure 8 shows a finite element simulation designed to verify the dynamic aspects of the equivalent model, including the microinertial terms. The figure shows a mesh for an explicit FE simulation of the impact of a flyer on a 100 configuration of octet unit cells. Inflow boundary conditions represent a massive flyer compared to the truss structure. The boundary conditions in the off-impact directions constrain the model to uniaxial deformation. The case of interest here is wave propagation in a semi-infinite medium. Therefore these results only consider the time before the elastic wave reaches the back face boundary conditions. The FE simulations were run with ALE3D, an arbitrary Lagrangian-Eulerian finite element code developed at Lawrence Livermore National Laboratory (Nichols, 2014).

Figure 9 compares the FE results, at several different impact velocities v, to the equivalent continuum model developed in this work. The initial relative density of the lattice material is $\bar{\rho} = 0.1$ for both the FE simulation and the continuum model. This figure shows a particle velocity-strain Hugoniot curve, so that the slope of the Rankine line connecting any two points on the Hugoniot gives the shock speed. In the FE models two approximately steady shocks develop. For each of these two shocks the combination of a wavespeed and a

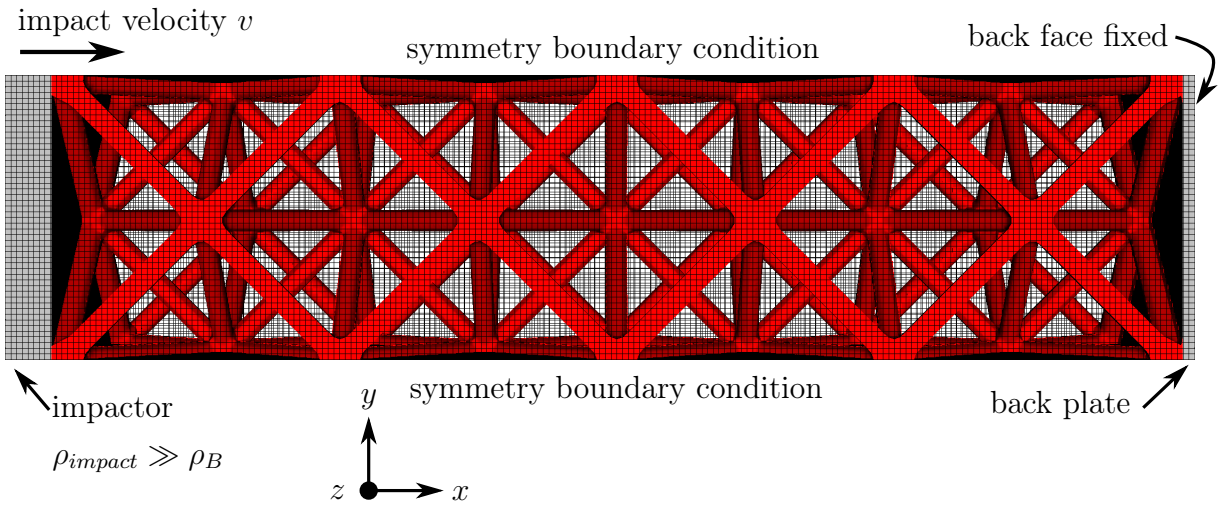

Figure 8: Eulerian finite element mesh used to verify the equivalent continuum model under impact loading. Impact occurs in the $+x$ direction, with symmetry boundary conditions on the top and bottom y and z faces of the model. Inflow boundary conditions represent a massive impactor compared to the truss. The end of the back plate is fixed. Mesh contains approximation 1 million elements.

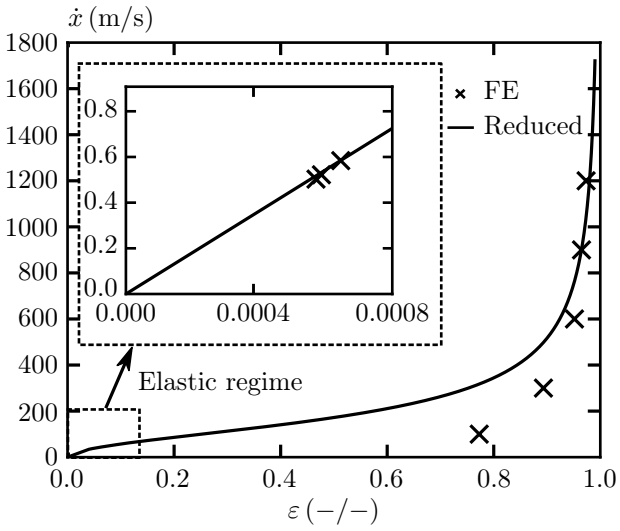

Figure 9: The $\dot{x}$-ε Hugoniot for planar impact of an infinite octet truss in the 100 direction. Relative density $\bar{\rho} = 0.1$. Figure compares the FE simulation results to the equivalent continuum model.

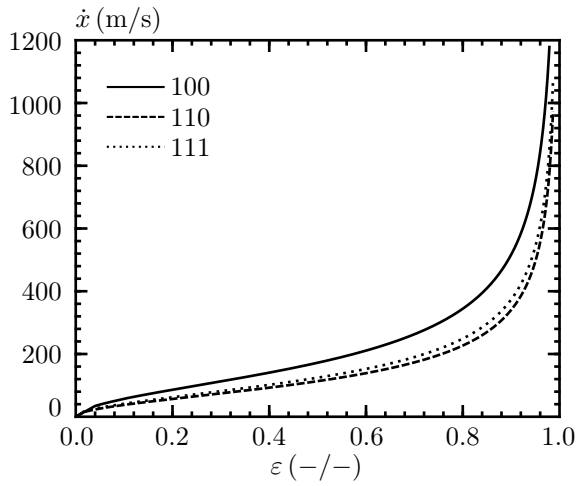

Figure 10: $\dot{x}$-ε Hugoniot curves for planar impact of an infinite octet truss in three different directions: 100, 110, and 111. Initial relative density $\bar{\rho} = 0.1$.

final particle speed produces a single point on the Hugonoit. The coordinates of this point can be constructed via the Rankine-Hugoniot conditions. For the continuum material model a simple python script directly solves the nonlinear equations representing the Rankine-Hugoniot conditions for the unknown shock speed c and final strain ε^+ given the initial state ε^- and $\dot{x}^-$ and final particle velocity $\dot{x}^+$:

$$\begin{aligned} \dot{x}^+ - \dot{x}^- = & \quad c\left(\varepsilon^- - \varepsilon^+\right) \\ \sigma\left(\varepsilon^+\right) - \sigma^- = & \quad \rho_I \bar{\rho} c^2 \left(\varepsilon^+ - \varepsilon^-\right). \end{aligned} \tag{54}$$

Here, $\sigma\left(\varepsilon^+\right)$ represents the equivalent continuum material model developed in this work subjected to axial strain in the direction of interest. Solving Eq. 54 then requires inverting the nonlinear stress-strain relation. The term ρ_I represents the effective inertial density of the truss, accounting for microinertial effects. For the octet, as shown above, $\rho_I = \frac{1}{3}\rho_B$.

As Figure 9 indicates, the effective truss behaves elasto-plastically with the bilinear Hugoniot reflecting the elastic-to-plastic transition (Davison, 2008). The transition point between elastic and plastic response is called the Hugoniot elastic limit (HEL). In the finite element model this means for impactor speeds above $\dot{x}_{HEL}$ two shocks propagate through the simulation: an initial elastic precursor wave, with wavespeed equal to the elastic sound speed of the effective material, followed by a plastic compaction wave. Therefore, each simulation produces two data points on the Hugonoit: the elastic limit, reflecting the properties of the elastic precursor, and a final point, reflecting the properties of the compaction wave. Similarly, care must be taken when solving Eq. 54 for the continuum model. For final particle velocities $\dot{x}^+$ less than $\dot{x}_{HEL}$ the initial state of the material is quiescent: $\dot{x}^- = 0$ and $\varepsilon^- = 0$. For particle velocities above the elastic limit, the initial state of the material is at the HEL: $\dot{x}^- = \dot{x}_{HEL}$ and $\varepsilon^- = \varepsilon_{HEL}$.

In the elastic regime, the continuum Hugoniot curve lies on the HEL points extracted from the finite element simulation. This means the equivalent model reproduces the elastic sound speed observed in the FE simulations. However, as the impact velocity increases the continuum model becomes less accurate. Detailed observation of the FE simulation results reveals three factors affecting the accuracy of the continuum model:

1. At moderate impact velocities the compaction wave significantly displaces the truss joint positions. Extending the continuum model to large deformations by allowing the coordinates of the joints to deform with the overall material deformation would eliminate this source of error.
2. At higher impact velocities struts can fail in bending by dynamic buckling. The model does not account for this mode of deformation.
3. Finally, at very high impact velocities the entire truss structure substantially collapses at the compaction shock front. The material around the compaction shock no longer resembles a periodic truss but rather a solid with dispersed voids. The mechanics of the model described here do not account for this behavior.

Despite these shortcomings, the equivalent continuum model does approximately reproduce the main features of the Hugoniot curve extracted from the FE simulation. In particular, and especially at high impact velocities, the compaction wavespeeds calculated from the FE results and the wavespeeds computed from the continuum model closely match. Furthermore, in the elastic regime the continuum model agrees with the FE results. Neglecting microinertial effects, for example, by using the physical density $\bar{\rho}\rho_B$ in place of the effective inertial density $\bar{\rho}\rho_I$ results in significant errors between the equivalent continuum model and the finite element results in the elastic regime – even though as Section 4.1 demonstrates the effective elastic tensor exactly reproduces the quasi-static elastic response of the discrete structure.

Figure 10 shows the effect of impact direction on the Hugoniot curve. Plastic and elastic anisotropy have a significant influence on model behavior. For example, the 100 Hugoniot curve varies substantiality from the 110 and 111 direction curves. The elastic sound speed also varies with the direction of impact, reflecting the cubic anisotropy of the effective stiffness tensor.

5. Conclusions

The key contributions of this work are:

- An equivalent continuum model for periodic truss structures that includes dynamic effects and verification of the model against detailed finite element simulations. The continuum model is most accurate for trusses with low relative densities, at low levels of deformation, and low impact velocities. However, it provides reasonable accuracy even at the higher levels of deformation associated with shock loading.

- For simple lattices, the expression for the axial stress resolved in each strut preserves joint equilibrium under arbitrary loadings, an improvement over previous models.

- Overcoming the problem of vertices on the equivalent truss yield surface by incorporating moderate rate sensitivity. Crystal plasticity models inspire this solution. The work draws other connections between crystal plasticity and equivalent truss models. These connections develop because both types of models describe lattice materials.

- A novel expression for the inertial body force of a periodic truss that correctly accounts for microinertial effects. Accurate calculation of dynamic properties, even long wavelength characteristics such as the elastic sound speed, requires these microinertial corrections in addition to the correct effective elastic stiffness tensor.

The equivalent continuum model developed here is suitable for implementation as a standard material model in a finite element code. Such an implementation can correctly handle boundary effects and more general loadings than the verification examples presented here. For simple lattices, the small deformation model described in this work also easily extends to large deformations via a process analogous to how crystal plasticity models extend to large lattice deformations.

Acknowledgements

References

Asaro, R. J., 1983. Micromechanics of crystals and polycrystals. In: Adv. Appl. Mech. Vol. 23. pp. 1–115.

Bishop, J., Hill, R., Jun. 1951a. A theoretical derivation of the plastic properties of a polycrystalline face-centred metal. Philos. Mag. 42 (334), 1298–1307.

Bishop, J., Hill, R., Jul. 1951b. A theory of the plastic distortion of a polycrystalline aggregate under combined stresses. Philos. Mag. 42 (327), 414–427.

Davison, L., 2008. Fundamentals of shock propagation in solids.

Deshpande, V., Fleck, N., Ashby, M., Aug. 2001. Effective properties of the octet-truss lattice material. J. Mech. Phys. Solids 49 (8), 1747–1769.

Elsayed, M. S., Pasini, D., Jul. 2010. Multiscale structural design of columns made of regular octet-truss lattice material. Int. J. Solids Struct. 47 (14-15), 1764–1774.

Evans, A., Hutchinson, J., Fleck, N., Ashby, M., Wadley, H., Jan. 2001. The topological design of multifunctional cellular metals. Prog. Mater. Sci. 46 (3-4), 309–327.

Fish, J., Chen, W., Nagai, G., May 2002a. Non-local dispersive model for wave propagation in heterogeneous media: multi-dimensional case. Int. J. Numer. Methods Eng. 54 (3), 347–363.

Fish, J., Chen, W., Nagai, G., May 2002b. Non-local dispersive model for wave propagation in heterogeneous media: one-dimensional case. Int. J. Numer. Methods Eng. 54 (3), 331–346.

Fish, J., Filonova, V., Kuznetsov, S., Sep. 2012. Micro-inertia effects in nonlinear heterogeneous media. Int. J. Numer. Methods Eng. 91 (13), 1406–1426.

Forest, S., Pilvin, P., 1999. Modelling finite deformation of polycrystals using local objective frames. Zeitschrift fuer Angew. Math. und Mech. 79, 199–202.

Fuller, R. B., 1961. Octet truss.

Hill, R., Rice, J., Dec. 1972. Constitutive analysis of elastic-plastic crystals at arbitrary strain. J. Mech. Phys. Solids 20 (6), 401–413.

Howard, S. M., Pao, Y.-H., Aug. 1998. Analysis and Experiments on Stress Waves in Planar Trusses. J. Eng. Mech. 124 (8), 884–891.

Hutchinson, R., Fleck, N., Apr. 2006. The structural performance of the periodic truss. J. Mech. Phys. Solids 54 (4), 756–782.

Johnston, S. R., Rosen, D. W., Reed, M., Wang, H. V., 2006. Analysis of mesostructure unit cells comprised of octet-truss structures. In: Proc. Seventeenth Solid Free. Fabr. Symp. Austin, TX.

Kocks, U. F., 1998. Kinematics and Kinetics of Plasticity. In: Kocks, U. F., Tome, C. N., Wenk, H.-R. (Eds.), Texture and Anisotropy. Ch. 8, pp. 327–389.

Kruth, J.-P., Leu, M., Nakagawa, T., Jan. 1998. Progress in additive manufacturing and rapid prototyping. CIRP Ann. - Manuf. Technol. 47 (2), 525–540.

Martinsson, P.-G., Babuška, I., May 2007. Mechanics of Materials with Periodic Truss or Frame Micro-Structures. Arch. Ration. Mech. Anal. 185 (2), 201–234.

Messner, M. C., Beaudoin, A. J., Dodds, R. H., 2015. Consistent crystal plasticity kinematics and linearization for the implicit finite element method. Eng. Comput. In press.

Mohr, D., Jun. 2005. Mechanism-based multi-surface plasticity model for ideal truss lattice materials. Int. J. Solids Struct. 42 (11-12), 3235–3260.

Murr, L. E., Gaytan, S. M., Ramirez, D. A., Martinez, E., Hernandez, J., Amato, K. N., Shindo, P. W., Medina, F. R., Wicker, R. B., Jan. 2012. Metal fabrication by additive manufacturing using laser and electron beam melting technologies. J. Mater. Sci. Technol. 28 (1), 1–14.

Nichols, A., 2014. ALE3D User's Manual. Tech. rep., Lawrence Livermore National Laboratory.

Pao, Y.-h., Keh, D.-c., Howard, S. M., 1999. Dynamic response and wave propagation in plane trusses and frames. AIAA J. 37 (5), 594–603.

Rosen, D. W., Jan. 2007. Computer-aided design for additive manufacturing of cellular structures. Comput. Aided. Des. Appl. 4 (5), 585–594.

Roters, F., Eisenlohr, P., Hantcherli, L., Tjahjanto, D., Bieler, T., Raabe, D., Feb. 2010. Overview of constitutive laws, kinematics, homogenization and multiscale methods in crystal plasticity finite-element modeling: Theory, experiments, applications. Acta Mater. 58 (4), 1152–1211.

Signorelli, J., von Flotow, A., Oct. 1988. Wave propagation, power flow, and resonance in a truss beam. J. Sound Vib. 126 (1), 127–144.

Srikantha Phani, A., Woodhouse, J., Fleck, N. A., 2006. Wave propagation in two-dimensional periodic lattices. J. Acoust. Soc. Am. 119 (4), 1995–2005.

Wang, Z.-P., Sun, C., Oct. 2002. Modeling micro-inertia in heterogeneous materials under dynamic loading. Wave Motion 36 (4), 473–485.

Warren, W., Kraynik, A., Mar. 1987. Foam mechanics: the linear elastic response of two-dimensional spatially periodic cellular materials. Mech. Mater. 6 (1), 27–37.

Winter, R. E., Cotton, M., Harris, E. J., Maw, J. R., Chapman, D. J., Eakins, D. E., McShane, G., Mar. 2014. Plate-impact loading of cellular structures formed by selective laser melting. Model. Simul. Mater. Sci. Eng. 22 (2), 025021.

Yong, Y., Lin, Y., Jul. 1992. Dynamic response analysis of truss-type structural networks: A wave propagation approach. J. Sound Vib. 156 (1), 27–45.

Zheng, X., Lee, H., Weisgraber, T. H., Shusteff, M., DeOtte, J., Duoss, E. B., Kuntz, J. D., Biener, M. M., Ge, Q., Jackson, J. a., Kucheyev, S. O., Fang, N. X.,

Spadaccini, C. M., Jun. 2014. Ultralight, ultrastiff mechanical metamaterials. Science (80-.). 344, 1373–1377.

A. Material Jacobian

Algorithm 1 poses the material model developed in this work as the solution to a set of nonlinear residual equations $\mathbf{R}_{n+1} = \mathbf{0}$. Solving these equations via the Newton-Raphson method requires the Jacobian matrix $\partial \mathbf{R}_{n+1}/\partial \mathbf{x}_{n+1}$, where $\mathbf{x}_{n+1}$ is the vector of unknown variables, here $\left[\begin{array}{ccc} \boldsymbol{\sigma}_{n+1} & \bar{\sigma}_{n+1} & \bar{\rho}_{n+1} \end{array} \right]^T$, with $\boldsymbol{\sigma} = \left[\begin{array}{cccccc} \sigma_{xx} & \sigma_{yy} & \sigma_{zz} & \sigma_{yz} & \sigma_{xz} & \sigma_{xy} \end{array} \right]^T$. Based on the structure of the residual equations the Jacobian matrix divides into blocks of the form

$$\mathbf{J} = \left[\begin{array}{ccc} \mathbf{J}_{11} & \mathbf{J}_{12} & \mathbf{J}_{13} \\ \mathbf{J}_{21} & J_{22} & J_{23} \\ \mathbf{J}_{31} & J_{32} & J_{33} \end{array} \right].$$

The following equations give each block:

$$\mathbf{J}_{11} = (1 + \operatorname{tr} \Delta\boldsymbol{\varepsilon}^p)\, \mathbf{I} + \frac{n\Delta\varepsilon_0}{\bar{\sigma}^n \bar{\rho}} \boldsymbol{\sigma} \otimes \left\{ \sum_{i=1}^{n_{bars}} |\sigma_i|^{n-1} \hat{\mathbf{C}}^{-1} \cdot (\mathbf{n}_i \otimes \mathbf{n}_i) \right\} + \frac{En\Delta\varepsilon_0}{\bar{\sigma}^n} \hat{\mathbf{C}} \cdot \left[\sum_{i=1}^{n_{bars}} |\sigma_i|^{n-1} (\mathbf{n}_i \otimes \mathbf{n}_i) \otimes \left\{ \hat{\mathbf{C}}^{-1} \cdot (\mathbf{n}_i \otimes \mathbf{n}_i) \right\} \right]$$

$$\mathbf{J}_{12} = -\frac{n}{\bar{\sigma}} \left(\boldsymbol{\sigma} \sum_{i=1}^{n_{bars}} \Delta\varepsilon_i + \bar{\rho} E \hat{\mathbf{C}} \cdot \Delta\boldsymbol{\varepsilon}^p \right)$$

$$\mathbf{J}_{13} = -\boldsymbol{\sigma} \frac{n}{\bar{\rho}} \sum_{i=1}^{n_{bars}} \Delta\varepsilon_i - E\hat{\mathbf{C}} \cdot (\Delta\boldsymbol{\varepsilon} - \Delta\boldsymbol{\varepsilon}^p) - nE\hat{\mathbf{C}} \cdot \Delta\boldsymbol{\varepsilon}^p$$

$$\mathbf{J}_{21} = -\frac{Hn\Delta\varepsilon_0}{\bar{\sigma}^n \bar{\rho}} \sum_{i=1}^{n_{bars}} |\sigma_i|^{n-2} \sigma_i \hat{\mathbf{C}}^{-1} \cdot (\mathbf{n}_i \otimes \mathbf{n}_i)$$

$$J_{22} = 1 + \frac{Hn}{\bar{\sigma}} \sum_{i=1}^{n_{bars}} |\Delta\varepsilon_i|$$

$$J_{23} = \frac{Hn}{\bar{\rho}} \sum_{i=1}^{n_{bars}} |\Delta\varepsilon_i|$$

$$\mathbf{J}_{31} = \frac{n\Delta\varepsilon_0}{\bar{\sigma}^n} \sum_{i=1}^{n_{bars}} |\sigma_i|^{n-1} \hat{\mathbf{C}}^{-1} \cdot (\mathbf{n}_i \otimes \mathbf{n}_i)$$

$$J_{32} = -\frac{n\bar{\rho}}{\bar{\sigma}} \sum_{i=1}^{n_{bars}} \Delta\varepsilon_i$$

$$J_{33} = 1 + \operatorname{tr} \Delta\boldsymbol{\varepsilon}^p - n \sum_{i=1}^{n_{bars}} \Delta\varepsilon_i.$$

In these expressions $\Delta\varepsilon_i = \dot{\varepsilon}_i \Delta t = \Delta\varepsilon_0 \left| \frac{\sigma_i}{\bar{\sigma}_i} \right|^{n-1} \frac{\sigma_i}{\bar{\sigma}_i}$.

This work performed under the auspices of the U.S. Department of Energy by Lawrence Livermore National Laboratory under Contract DE-AC52-07NA27344.